Electrochemical Reaction Kinetics for CO-CO_2 Electrochemical Conversion in the Nickel-Patterned Electrode

Yu Luo[a], Yixiang Shi[a], Wenying Li[a,b], Ningsheng Cai[a]
a. Key Laboratory for Thermal Science and Power Engineering of Ministry of Education, Department of Thermal Engineering, Tsinghua University, Beijing 100084, China
b. Sichuan Energy Internet Research Institute, Tsinghua University, Sichuan 610213, China

1 High-temperature CO-CO_2 electrochemical conversion

Reversible solid oxide cells (RSOC) can operate in both solid oxide fuel cell (SOFC) and solid oxide electrolysis cell (SOEC) modes at a high temperature of 600-1000°C. The high operating temperature enables RSOC to effectively utilize CO to produce electricity in SOFC mode or electrolyze CO_2 to CO even methane by reacting with H_2/H_2O in SOEC mode. Therefore, RSOC has the advantages of seasonal energy storage, CO_2 emission reduction, and fast reaction kinetics. Abundant researches on the SOFC mode can be found. The researches on SOEC has just arisen in the recent years because of its potential application in the area of the renewable energy and nuclear energy[1]. More attention is paid on the performance, materials and stability in the atmosphere of H_2/H_2O due to better electrochemical performance rather than CO/CO_2. Nevertheless, CO/CO_2 is the necessary species for the application of carbon dioxide emission reduction. Currently, the researches on the electrochemical conversion of RSOC in the atmosphere CO/CO_2 were mainly based on the porous electrode structure of the Ni-YSZ(yttria stabilized zirconia)[3]-[7]. It's noticed that carbon deposition could be one of the significant problems has to be considered in the atmosphere of CO/CO_2[5]. A series of reversible or irreversible harmful effects on the fuel electrode of RSOC could be caused by carbon deposition. In the common fuel electrode materials of nickel/yttria stabilized zirconia(Ni-YSZ), catalyst deactivation, porosity decrease and performance degradation can cause the reversible detrimental effects due to occupying reaction active sites[8], irreversible detrimental effects are mainly contributed to nickel dusting and fibers growing[8]. These damages lead to the limitation of the carbonaceous gas application for RSOC. Researches on the carbon deposition in the SOFC fueled with CH_4 or other hydrocarbon fuels have been carried out[9]-[11]. However, carbon deposition in the atmosphere of CO/CO_2 might be different, especially for SOEC mode. In this study, the mechanism of CO-CO_2 electrochemical reduction was proposed and the rate-determining steps were analyzed based on the analytical calculation to understand the relation between the electrochemical pathway and carbon deposition/consumption.

Correspondence to: Yixiang Shi shyx@tsinghua.edu.cn

2 Nickel-patterned electrode

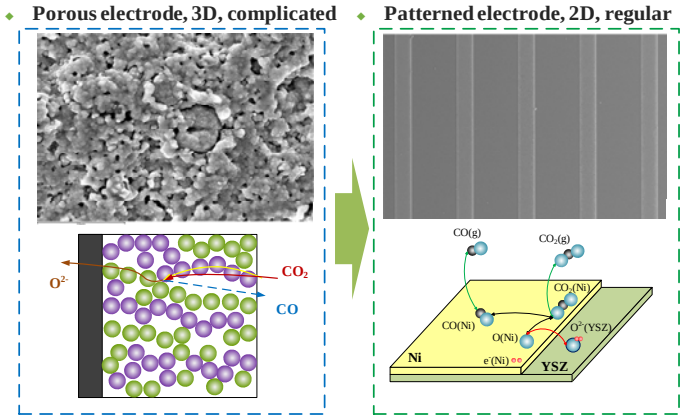

Figure 1. Comparison between porous and patterned electrodes

Triple-phase boundary (TPB) is widely believed to be the electrochemical reaction active sites. Besides, the adsorption/desorption and surface reaction could occur on the surface of Ni and YSZ. The Ni-YSZ electrode is fabricated by the co-sintering of the Ni and YSZ particles to form a three-dimension complicated porous structure. Such a complicated structure not only prevents researchers from the accurate estimation and surface characterization of the effective reaction active sites but also makes it hard to separate the effects of chemical reaction, electrochemical reaction and bulk gas diffusion. To simplify the porous structure, the patterned electrode is convinced to be an appropriate tool to identify the reaction kinetics of the RSOC, which is a dense and ultrathin pure-metal electrode with a regulable shape. The quasi-two-dimension structure of the Ni-patterned electrode enables researchers to quantify the TPB length and Ni surface area, exclude the effect of bulk gas diffusion and separate the active regions of the chemical/electrochemical reactions. As the right photo of Figure 1 shows, the dark region is the single crystal YSZ electrolyte and the light region is the Ni stripes. Our group has tested the 800 nm-thickness Ni-patterned electrodes with the purity of 99.999%, which was magnetron-sputtered on the surface of the single crystal 13 mol% YSZ electrolytes with the surface roughness Ra of 0.69 nm. The TPB length of the Ni-patterned electrode was quantified to be 364.3±0.6 nm, Ni area to be 19.07±0.09 mm^2 and TPB density to be 19.10 mm mm^{-2}. More details can be found in our previous papers[8]-[12].

3 Electrochemical reaction kinetics

Previous research[12] has published the experimental data of the Ni-patterned electrode in the atmosphere of CO-CO_2. The electrochemical reaction kinetics can be described by the Bulter-Volmer (B-V) equation:

$$i = i_0 \left[\exp\left(\frac{\alpha_{an} n_e F \eta}{RT} \right) - \exp\left(-\frac{(1-\alpha_{an}) n_e F \eta}{RT} \right) \right] \quad (1)$$

Where i, i_0 denote the current density and exchange current density, α_{an} the anodic charge transfer coefficient of the global reaction, F the Faraday constant, R the universal gas constant, T temperature, n_e the number of electron transfer in the electrochemical reaction (n_e=2 here). i_0 can be expressed in the Arrhenius form[12]:

$$i_0 = \gamma \left(pCO \right)^a \left(pCO_2 \right)^b \exp\left(-\frac{E_{act}}{RT} \right) \quad (2)$$

Here, the exponential factor a, b and activation energy E_{act} are the key parameters of the electrochemical reaction kinetics in the CO-CO_2 atmosphere. In Ref. [12], the polarization curves at the different partial pressure of CO (pCO), CO_2(pCO_2) and temperature were measured, based on which the polarization resistance at open-circuit voltage (OCV) $R_{pol,OCV}$ was calculated. $R_{pol,OCV}$ was proportional to $1/i_0$. Thus, $R_{pol,OCV}$ should be proportional to the log pCO (napierian logarithm of pCO), log pCO_2 and $1/T$. The values of a, b, E_{act} can be derived from the slope of the linear fitting $R_{pol,OCV}$ - log pCO, $R_{pol,OCV}$ - log pCO_2 and $R_{pol,OCV}$ – $1/T$ curves, respectively. Ref.[12] reports that a=0.657, b=0.011, E_{act}=1.77 eV, which means the i_0 improved with pCO increasing but changed little with pCO_2. In addition, carbon deposition on the Ni-patterned electrode was also characterized in Ref.[8], which found the carbon element in the middle of the Ni stripes was lower than near TPB in SOFC mode but higher than that in SOEC mode. According to this phenomenon, Ref.[8] speculated an electrochemical reaction pathway related to carbon deposition:

$$C(Ni)+O^{2-}(YSZ)\underset{SOEC}{\overset{SOFC}{\rightleftharpoons}}CO(Ni)+(YSZ)+2e^{-} \quad (3)$$

Presently, oxygen splitting was widely considered as the patterned reaction mechanism for the fuel electrode of RSOC in the CO-CO_2 atmosphere[16]. The proposed patterned elementary reaction mechanism in the existing papers has been proposed as Table 1[16].

Table 1: Patterned reaction mechanism in the CO-CO_2 atmosphere [16]

Adsorption and desorption on the Ni surface	
$CO_2(g)+(Ni) \leftrightarrow CO_2(Ni)$	R1
$CO(g)+(Ni) \leftrightarrow CO(Ni)$	R2
Surface reaction on the Ni surface	
$CO_2(Ni)+(Ni) \leftrightarrow CO(Ni)+O(Ni)$	R3
$CO(Ni)+(Ni) \leftrightarrow C(Ni)+O(Ni)$	R4
Charge transfer at TPB	
$O(Ni)+(YSZ)+2e^{-} \underset{SOFC}{\overset{SOEC}{\rightleftharpoons}} (Ni)+O^{2-}(YSZ)$	R5
Transfer of oxygen ions between the surface and bulk of YSZ	
$O^{2-}(YSZ)+V_O^{\cdot\cdot}(YSZ) \leftrightarrow O_O^{\times}(YSZ)+(YSZ)$	R6

4 Analytical calculation

It has reported that CO_2 only physisorbed and is hard to chemisorb on the surface of pure transient metal at a temperature of 80-100 K[13]. Ref. [14] also indicates CO_2 chemisorption on the surface of the pure transient metal requires some special conditions, such as the alkali metal modification, surface defects and atomic arrangement disorder on the metal surface. Nevertheless, CO adsorption was thought to be more significant[7]-[15]. Existing elementary reaction models[5]-[7],[16]-[18] also indicate CO(Ni) and (Ni) are the major surface element on the Ni surface. Thus, it's reasonable to assume R4 is non-ignorable and even contributes more to O(Ni) production than R3 on the pure-Ni surface especially in SOEC mode. To evaluate how important role the carbon deposition plays on the reactions on the surface of the Ni-patterned electrode, the analytical calculation was performed according to the Ref.[19],[20] by assuming different reaction rate-limiting steps. First of all, the only reaction R4 related to carbon is neglected and R1-3, R5-6 are considered. By respectively assuming R1-R3 or R4 as the rate-limiting reaction, the exchange current density can be experissed in Table 2 according to the analytical calculation. Here, when one reaction was assumed to be rate-limiting, the others reaction was considered to be at the equilibrium state. The surface diffusion was neglected, the total surface coverage of CO(Ni) and (Ni) was assumed to be 1 and surface coverage of $O_O^{\times}$(YSZ) and $V_O^{\cdot\cdot}$(YSZ) assumed to be constant. In Table 2, K_i is the reaction equilibrium constant of reaction Ri, k_{if} the forward reaction kinetic constant, E_{an} the electric potential between Ni and YSZ, β_{an} the

anodic charge transfer coefficient of the reaction R5 (a value between 0 and 1). Table 2 shows except for R2 as rate-limiting, i_0 has a negative correlation with pCO, which is opposite to the experimental results [8]. Even when R2 was assumed as the rate-limiting reaction, the value of a in Eq.(2) is equal to 1, larger than the value in Ref. [8].

Table 2: Key reaction kinetic parameters in B-V equation for the CO-CO_2 atmosphere

Rate-limiting reaction	$i_0\left(\propto pCO^a pCO_2{}^b, Exp: a=0.657, b=0.011\right)$	Factor λ (Independent on pCO/pCO_2)	α_{an}
R1	$i_0 = \lambda \dfrac{pCO_2}{1/K_2 + pCO}$	$-\dfrac{2FS_{Ni}k_{1f}}{K_2}$	1
R2	$i_0 = \lambda \dfrac{pCO}{\dfrac{\exp\left(2FE_{an}^{eq}/RT\right)}{K_1K_3K_5K_6} + pCO_2}$	$-\dfrac{2FS_{Ni}k_{2f}}{K_1K_3K_5K_6\exp\left(2FE_{an}^{eq}/RT\right)}$	0
R3	$i_0 = \lambda \dfrac{pCO_2}{\left(1/K_2 + pCO\right)^2}$	$-\dfrac{2FS_{Ni}k_{3f}}{K_1K_2^2}$	1
R5	$i_0 = \lambda \dfrac{pCO_2{}^{\beta_{an}}}{pCO^{\beta_{an}}\left(1/K_2 + pCO\right)}$	$-\dfrac{2Fl_{TPB}k_{5f}}{K_5^{1-\beta_{an}}\left(1+K_6\right)}K_1^{\beta_{an}}K_2^{1+\beta_{an}}K_3^{\beta_{an}}K_6^{3-\beta_{an}}$	β_{an}

Table 3: Simplified patterned reaction mechanism in the CO-CO_2 atmosphere

Adsorption and desorption on the Ni surface	
CO(g)+(Ni) $\leftrightarrow$ CO(Ni)	R2
C(s)+(Ni) $\leftrightarrow$ C(Ni)	R7
Charge transfer at TPB	
CO(Ni)+(YSZ)+2e$^-$ $\underset{\text{SOFC}}{\overset{\text{SOEC}}{\rightleftharpoons}}$ C(Ni)+O^{2-}(YSZ)	R8
CO_2(g)+(YSZ)+2e$^-$ $\underset{\text{SOFC}}{\overset{\text{SOEC}}{\rightleftharpoons}}$ CO(Ni)+O^{2-}(YSZ)	R9
Transfer of oxygen ions between the surface and bulk of YSZ	
O^{2-}(YSZ)+$V_O^{\cdot\cdot}$(YSZ) $\leftrightarrow$ $O_O^{\times}$(YSZ)+(YSZ)	R6

Further, the carbon deposition reaction R4 was considered. Considering ignorable CO_2(Ni)/O(Ni) and fast CO_2 desorption, the patterned mechanism was simplified as Table 3. R8 and R9 are two separated charge transfer reactions when CO and CO_2 are both fed to the Ni electrode. When one of them was assumed as the rate-limiting reaction, the other one was neglected to estimate their respective effect on the exchange current density. The results of the analytical calculation were shown in Table 4. Here, β_{an}, β_{ca} are the anodic and cathodic charge transfer coefficient and their sum is equal to 1.

Table 4: Key reaction kinetic parameters in B-V equation when R7 was assumed to be rate-limiting

Rate-limiting reaction	$i_0\left(\propto pCO^a pCO_2{}^b, Exp: a=0.657, b=0.011\right)$	Factor λ (Independent on pCO/pCO_2)	α_{an}
R2 (Ignoring R9)	λpCO	$-\dfrac{2FS_{Ni}k_{2f}K_6K_8}{K_6K_8 + K_7\exp\left(2FE_{an}^{eq}/RT\right)}$	1
R2 (Ignoring R8)	$\lambda \dfrac{pCO}{\dfrac{\exp\left(2FE_{an}^{eq}/RT\right)}{K_1K_3K_5K_6} + pCO_2}$	$-\dfrac{2FS_{Ni}k_{2f}}{K_1K_3K_5K_6\exp\left(2FE_{an}^{eq}/RT\right)}$	0

R8	$\lambda \frac{pCO^{\beta_{an,R8}}}{1/K_2 + pCO}$	$-\frac{2Fl_{TPB}k_{8f}K_6^{\beta_{an,R8}}K_7^{1-\beta_{an,R8}}}{K_2^{2-\beta_{an,R9}}K_8^{1-\beta_{an,R9}}(1+K_6)}$	$\beta_{an,R8}$
R9	$\lambda \frac{pCO^{\beta_{ca,R9}}\, pCO_2^{\beta_{an,R9}}}{(1/K_2 + pCO)^{\beta_{ca,R9}}}$	$-\frac{2Fl_{TPB}k_{9f}K_6^{\beta_{an,R9}}K_2^{\beta_{ca,R9}}}{K_9^{\beta_{ca,R9}}(1+K_6)}$	$\beta_{an,R9}$

The possible patterned reaction mechanism can be derived by analyzing the relation between i_0 and pCO/pCO_2. The surface coverage (Ni) was calculated to be large than but in the same order of magnitude as CO(Ni)[16]-[18]. When R8 was rate-limiting and (Ni) coverage is larger than CO(Ni) coverage, the variation trend of i_0 with pCO/pCO_2 was similar with the experiment[8]. When R9 was rate-limiting and the anodic charge transfer coefficient of R9 $\beta_{an,R9}$ was small enough, the variation of i_0 with pCO/pCO_2 also agreed well with experiment[8].

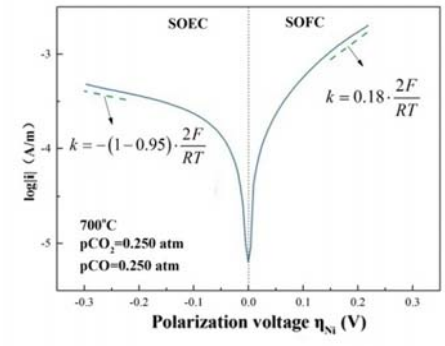

Figure 2. Polarization of the Ni-patterned electrode in SOEC/SOFC modes at 700ºC, $pCO=pCO_2=0.25$ atm[8]

4 Rate-limiting reactions for SOEC and SOFC modes

According to B-V equation (Eq.1), the slope of η_{Ni}-log|i| curve can approximately approaches to $2F\alpha_{an}/RT$ in SOFC mode and -2F (1-α_{an}) RT in SOEC mode when the overpotential is large enough. Different patterned reaction mechanism in SOEC and SOFC mode may lead to different values of α_{an}. The experimental curve in Figure 2 shows the value of α_{an} approaches to about 0.18 in SOFC mode and 0.95 in SOEC mode[8]. In consequence, carbon deposition/consumption was likely to be relevant to the electrochemistry in the Ni-patterned electrode, especially in SOEC mode. In SOFC mode, CO oxidation into CO_2 was more probably the major electrochemical reaction while adsorbed carbon also could be oxidated into CO. In SOEC mode, the reaction rate of R9 could be inhibited due to difficult CO_2 adsorption, hence, CO reduction into carbon could be more probably the major electrochemical reaction.

References

[1] Shi Y, Luo Y, Li W, Ni M, Cai N. (2015). High Temperature Electrolysis for Hydrogen or Syngas Production from Nuclear or Renewable Energy. Handbook of Clean Energy Systems. John Wiley & Sons, Ltd. (ISBN 978-1-118-99197-8).

[2] Ebbesen SD, Jensen SH, Hauch A, Mogensen MB. (2014). High temperature electrolysis in alkaline cells, solid proton conducting cells, and solid oxide cells. Chem. Rev. 114: 10697.

[3] Ebbesen SD, Mogensen M. (2009). Electrolysis of carbon dioxide in solid oxide electrolysis cells. J. Power Sources 193: 349.

[4] Zhan Z, Zhao L. (2010). Electrochemical reduction of CO_2 in solid oxide electrolysis cells. J. Power Sources 195: 7250.

[5] Shi Y, Luo Y, Cai N, Qian J, Wang S, Li W, Wang H. (2013). Experimental characterization and modeling of the electrochemical reduction of CO_2 in solid oxide electrolysis cells. Electrochim. Acta 88: 644.

[6] Shi Y, Li C, Cai N. (2011). Experimental characterization and mechanistic modeling of carbon monoxide fueled solid oxide fuel cell. J. Power Sources 196: 5526.

[7] Hanna J, Lee WY, Ghoniem AF. (2013). Kinetics of carbon monoxide electro-oxidation in solid-oxide fuel cells from Ni-YSZ patterned-anode measurements. J. Electrochem. Soc. 160: F698.

[8] Li W, Shi Y, Luo Y, Wang Y, Cai N. (2015). Carbon deposition on patterned nickel/yttria stabilized zirconia electrodes for solid oxide fuel cell/solid oxide electrolysis cell modes. J. Power Sources 276: 26.

[9] Li C, Shi Y, Cai N. (2013). Carbon deposition on nickel cermet anodes of solid oxide fuel cells operating on carbon monoxide fuel. J. Power Sources 225: 1.

[10] Gorte RJ, Vohs JM. (2011). Catalysis in solid oxide fuel cells. Annu Rev Chem Biomol Eng. 2: 9.

[11] Cimenti M, Hill JM. (2009). Direct utilization of ethanol on ceria‐based anodes for solid oxide fuel cells. Asia‐Pacific J. Chem. Eng. 4: 45.

[12] Li W, Shi Y, Luo Y, Wang Y, Cai N. (2016). Carbon monoxide/carbon dioxide electrochemical conversion on patterned nickel electrodes operating in fuel cell and electrolysis cell modes. Int. J. Hydrogen Energy 41: 3762.

[13] Burghaus U. (2014). Surface chemistry of CO_2-adsorption of carbon dioxide on clean surfaces at ultrahigh vacuum. Prog. Surf. Sci. 89: 161.

[14] Onsgaard J, Hoffmann SV, Møller P, Godowski PJ, Wagner JB, Paolucci G, Baraldi A, Comelli G, Groso A. (2003). Adsorption of CO_2 and Coadsorption of H and CO_2 on Potassium‐Promoted Cu (115). ChemPhysChem 4: 466.

[15] Sukeshini AM, Habibzadeh B, Becker BP, Stoltz CA, Eichhorn BW, Jackson GS. (2006). Electrochemical Oxidation of H_2, CO, and CO/H_2 Mixtures on Patterned Ni Anodes on YSZ Electrolytes. J. Electrochem. Soc. 153:A705.

[16] Janardhanan VM, Deutschmann O. (2006). CFD analysis of a solid oxide fuel cell with internal reforming: Coupled interactions of transport, heterogeneous catalysis and electrochemical processes. J. Power Sources 162: 1192.

[17] Li W, Shi Y, Luo Y, Cai N. (2013). Elementary reaction modeling of CO2/H2O co-electrolysis cell considering effects of cathode thickness. J. Power Sources 243: 118.

[18] Ong K, Hanna J, Ghoniem AF. (2017). Investigation of a Combined Hydrogen and Oxygen Spillover Mechanism for Syngas Electro-Oxidation on Ni/YSZ. J. Electrochem. Soc. 164: F32.

[19] Lee WY, Wee D, Ghoniem AF. (2009). An improved one-dimensional membrane-electrode assembly model to predict the performance of solid oxide fuel cell including the limiting current density. J. Power Sources 186: 417.

[20] Zhu H, Kee RJ, Janardhanan VM, Deutschmann O, Goodwin DG. (2005). Modeling elementary heterogeneous chemistry and electrochemistry in solid-oxide fuel cells. J. Electrochem. Soc. 152: A2427.